Prediction of high cycle fatigue in aluminum bond wires: A physics of failure approach combining experiments and multi-physics simulations

Jeroen Bielen, Jan-Joris Gommans, Frank Theunis
Philips Semiconductors –Innovation Centre for RF
Gerstweg 2, 6534AE Nijmegen, The Netherlands
E-mail: jeroen.bielen@philips.com

Abstract

Aluminum wire bonds, as used in a ceramic air cavity package for LDMOS, will intrinsically be prone to mechanical fatigue due to temperature and power cycling causing the wires to expand and shrink in a cyclical way. Under certain pulsed application conditions, the required amount of current cycles the product must survive is so high that not just low cycle fatigue, caused by cyclic plastic deformation, but also high cycle fatigue becomes a concern.

This paper describes how in-situ monitored power cycling experiments, using the Joule heating of the bond wires, were performed on dedicated test structures at different stress levels with wire loop shapes and test settings critical enough to find failures within reasonable test times. Wire bond settings were varied to create different amounts of initial damage as introduced by the plastic deformation of the heel and the wedge.

Finite element method was employed to calculate the stress amplitude in the heel of the bond wire in the experiments as function of current, pulse time and loop shape. This required a multi-physics approach using coupled electro-thermal and sequentially coupled thermo-mechanical simulations. The amount of initial damage was also estimated, using 2D FE simulations, in order to quantitatively take into account the initial plastic strains.

With the measured failure times (Nf) and calculated stress amplitude (S) the durability or S-N curves for different amounts of initial damage could be derived and fitted with the Basquin model. These fitted models were used to predict the expected lifetime for specified field conditions. Furthermore the models can be used to derive 'design for reliability rules' for wire loop shapes that will survive a specified user profile.

1. Introduction

For the next generation RF LDMOS devices used in e.g. base stations for mobile communication, aluminum metallization will be used to be compatible with standard CMOS manufacturing processes. In order to avoid well-known failure mechanisms originating from AuAl intermetallics (e.g. dry corrosion of $AlAu_4$ possibly catalyzed by halogens and/or Kirkendall voiding) and because of the high temperature that these products are operated at, aluminum needs to be used for the bond wires (Figure 1). To have flexibility in the wire loop shape, which is needed for RF design, wedge-wedge ultra sonic bonded aluminum wires will be used.

With the use of Aluminum wires in air cavity packages another reliability risk however rises: Mechanical fatigue of the wire due to power and temperature cycling (Figure 2), which will manifest itself in fracture of the heel of the bond wire (Figure 17). Depending on what is identified as a (power) cycle, the field conditions require between 10^4 and over 10^{10} cycles to failure (with failure probabilities <0.1%). This implies that, since aluminum has in general no endurance limit, even deformation well within the elastic range of the material may eventually lead to high-cycle fatigue failure.

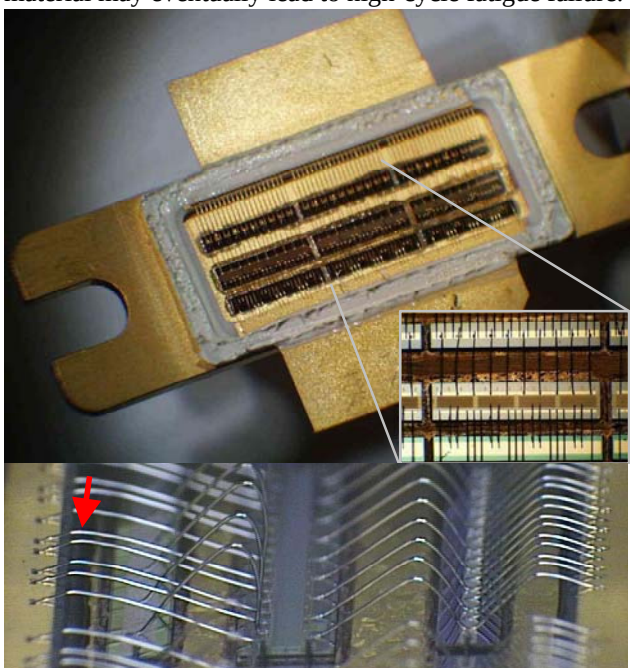

Figure 1: Example of an LDMOS product in air cavity package (ceramic cap removed) and detail of bond wires. Red arrow indicates the critical wire loop shapes that may be susceptible to power-cycling induced high-cycle fatigue.

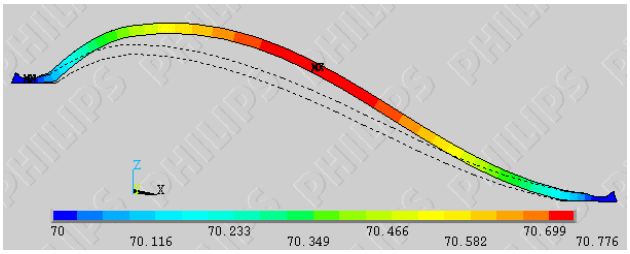

Figure 2: Joule heating will cause the bond wires to expand and contract in a cyclical manner, leading to mechanical fatigue

This paper describes how FE simulations have been used to project accelerated tests to user conditions in order to forecast the reliability in the field and come to a design for reliability. For that purpose a special test structure was put on a power cycle test where the current through the wire provided the mechanical stress by expansion of the wire due to the Joule heating. To derive the S-N curves (Basquin relation) the mechanical stress amplitude was estimated using coupled electro-thermal-mechanical FE simulations. It was found that, although the 2nd bonding angle was more critical, failure always occurred in the first bond. Therefore, an estimation of the plastic deformations, induced by the bonding process, was obtained from a 2D FE simulation. Experiments with different levels of these initial strains were performed in an attempt to find the dependency of the S-N curves on initial plastic strains.

To make this whole modeling approach of any practical use, the last step is the prediction of actual life under specified field conditions. In the given example, this has been done as function of 2 key design parameters, current and departure angle, to show how the model can be used to provide proper design rules that guarantee a design for reliability.

2. Method & Theory

Several relations have been proposed to relate cycles to failure to some damage metric, all of them being semi empirical. Most relations can be categorized as either strain based or energy based. Most common example of the first group is probably the Coffin-Manson relation using plastic strain range ε_p as damage metric to describe low-cycle fatigue:

$$Nf = C_1 \cdot (\Delta\varepsilon_p)^{-C_2} = \left(\frac{\Delta\varepsilon_p}{2 \cdot \varepsilon_f} \right)^{-C_2} \quad (1)$$

Nf is the number of cycles to 63% failures, C_1, C_2 & ε_f are material dependent constants. It is worthwhile to note that in the alternative of writing this relation, ε_f is actually the strain at fracture, the ultimate strain. This suggests that initial cold work i.e. plastic deformation, that effectively reduces the ultimate strain, will not affect the exponent c2, but only introduces a multiplication factor. Although it is not said that this will be the case for high-cycle fatigue, that takes place in the elastic strain range of the material, initial plastic strain may be expected to be relevant.

Although high cycle fatigue can be described by energy or strain based damage metrics as well, it is in general described by the Basquin equation, using stress amplitude as damage metric:

$$Nf = C_1 \cdot (\Delta\sigma)^{-C_2} = \left(\frac{\Delta\sigma}{2 \cdot \sigma_f} \right)^{-C_2} \quad (2)$$

Here, σ_f is the fracture stress (or sometimes the yield stress) of the material and although the fracture stress is not strongly affected by plastic deformation one might expect some effects also for high cycle fatigue. Another way to argue that cold work affects the durability by a certain factor, not changing the exponent, may be deduced from Miners rule that states that damage, defined as 1/Nf, from different loads over time, can be linearly super positioned. Although this law is intended for one single failure mode only, the initial deformation can be regarded as a severe strain cycle consuming a large part of the total life.

To study the effect of initial plastic deformation done by the bonding process on the durability relation, four different sets of process settings were used in the described experiments. All wires were stressed with a pulsed DC current, i.e. a power cycle test was conducted. The durability results of these different settings will be compared.

Most of the previously published results on aluminum bond wire fatigue deal with low cycle fatigue and the prediction of inelastic (plastic) strain range, which is used in the Coffin-Manson equation [1,3,4]. Very complete overview is reported in [5] where asymmetry in the bond wire is taken into account and some attention is paid to high cycle fatigue regime as well. Reported constants are c1=3.846e23 and c2=10.34 for 8mil wire but a verification on actual wires could not be conducted as another failure mode was reported to occur. We also found a transition from low to high cycle fatigue, between Nf=1-10K cycles, observable in a changing exponent in the power law relating strain and Nf. For our application the highest concern is however high cycle fatigue as this wear-out failure mode is not detectable by standard qualification tests while low-cycle fatigue is. Therefore, a physics of failure approach was used, in which this failure mode was isolated using dedicated test structures. For an extensive description of physics of failure approach see the work of Dasgupta [1].

Using joule heating as heating method of power cycling test has been described before and although an analytical equation of the heat transfer problem is readily available [3], in this case we have chosen to include the electro-thermal part in the FE modeling as this allows us to include temperature dependent material properties, and be more flexible in the boundary conditions & geometry (exact wire length does not need to be known and measured shapes can be used). The FE temperature responses did match the analytical ones.

In [4] the effect of the wire bond process settings is studied, however it is concluded that the effect of initial damage resulting in 0-hr or early failures are caused by the ultrasonic vibrations applied by the bonding process, and damage is not caused by the flexing of the wire as we found in this study.

3. Experimental

On a copper & ENIG plated substrate, 10 wire bonds were put in series. Parallel to each wire bond was a diode that would conduct the current when it's adjacent wire would fail. The substrate was mounted on a copper flange that was mounted on a forced convection cooled heat sink

(Figure 3). The heat sink was kept just above room temperature, which also ensures that no other failure mode, such as intermetallic corrosion or Kirkendall voiding will occur.

A test set-up was made that contained four of these modules, each stressed with a pulsed DC current. Used pulse length was between 10ms and 100ms, at a duty cycle of 50%, and was chosen such that the wire had sufficient time to heat-up, but have a frequency that still efficiently reduces the test time to find 70% of failures. Currents could be adjusted up to 2.5A, above that the diodes would start to conduct making the stress level of the wire inaccurate. For the calculations that follow, a correction for the diodes forward current has already been included for the currents between 2.2A and 2.5A

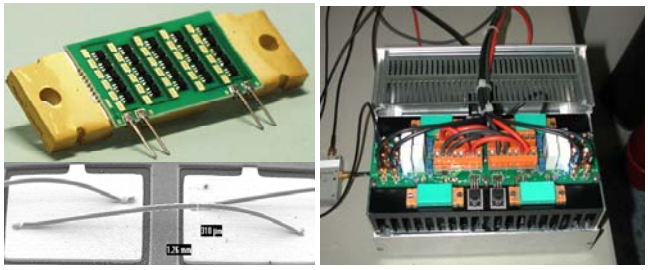

Figure 3: Test set-up and sample with 25 wire bonds in series.

The voltage across every module was monitored over time. Each time a wire would fracture, a distinct increase of the voltage would show up (Figure 15).

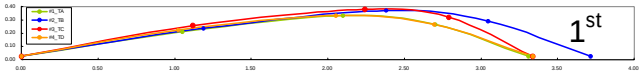

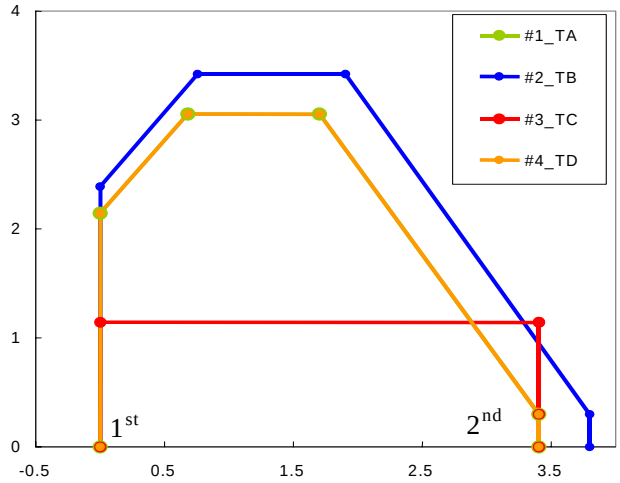

Figure 4: Four loop shapes were used in the experiments to create different initial plastic strains at the first heel (left bond). Bottom graph depicts the bond tool trajectories.

Four different loop shapes were used in the experiments to study the effect of the bond process (Figure 4). All loop shapes were chosen such that, based on the Hu-Dasgupta-Pecht model [6], they were expected to be critical enough to produce failures in reasonable test time. Loop #1 and #2 have identical shapes, 2 being larger, to have an implicit check on the simulations. Loop #3 has a different bond tool trajectory in order to induce different plastic strain at 0hr. Bond #4 is identical to #1, except that the wedge height is much thinner (50% of the reference thickness).

The different loop shapes were all put on at least four different stress levels, controlled by the current and the pulse time. Since the finally derived S-N curves would be used for extrapolation, the challenge was to find settings that would result in $Nf>10^7$.

4. FE model

The FE modeling efforts consisted of making two separate models: A 2D model was used to simulate the bonding process itself, in order to quantify the initial plastic strains in the bond. A 3D electro-thermal, sequentially coupled thermal-mechanical model was used to calculate the (average) stress and strain amplitudes during the actual tests. Both models were implemented in Ansys ^{TM}9.0.

2D Model

The 2D simulation was performed to estimate the amount of initial damage, evaluate the differences between first and second bond, and review its dependency on bond process settings. The model was a generalized plane strain 2D static large displacement simulation, comprising multiple contact pairs for the substrate and the bond tool and birth and death to model the 'sticking' of the bond. The bond tool geometry (radii) was based on suppliers CAD drawing. The bond tool trajectories depicted in Figure 4 were based on equipment settings. After the first load step in which the first wedge bond is made, fully bonded contact is switched on for the elements to the substrate based on a certain contact pressure of the adjacent already activated contact elements. The rest of the contact pairs have normal contact behavior. A friction coefficient of 0.5 was assumed and the contact penalty stiffness was lowered because of the large plastic deformations.

For the (lower order mesh of the) aluminum bond wire multi-lineair isotropic hardening, based on the measured monotonic stress-strain curves, was used (Figure 5). After completion of the 2nd bond in the simulation, an electro-thermal sequentially coupled mechanical simulation was also performed using mesh morphing to update the geometry. The wire geometry, however did not fully match the samples, and therefore this 2D model was not being used for the stress amplitude calculations. For those calculations, the measured actual loop geometry was used in the model.

3D Model

The ½ symmetry 3D model comprised a directly coupled electro-thermal transient simulation, followed by a sequentially coupled static thermo-mechanical model. Two different meshes were used for the different physics fields, so temperatures were interpolated from the thermal onto the mechanical mesh. As boundary conditions for the thermal model a fixed heat sink temperature on the bottom area of the flange and free convection ($10W/m^2K$)

on all other exposed surfaces was applied. The electro-thermal transient simulation was preceded by a steady state load step with 50% of the current to already reach a reasonable stable average temperature. The mechanical simulation was a static simulation in which the four consecutive pulses were simulated. For calculation of the stress, strain or temperature amplitude the last pulse was used to reach some stable temperature and stress-strain loop.

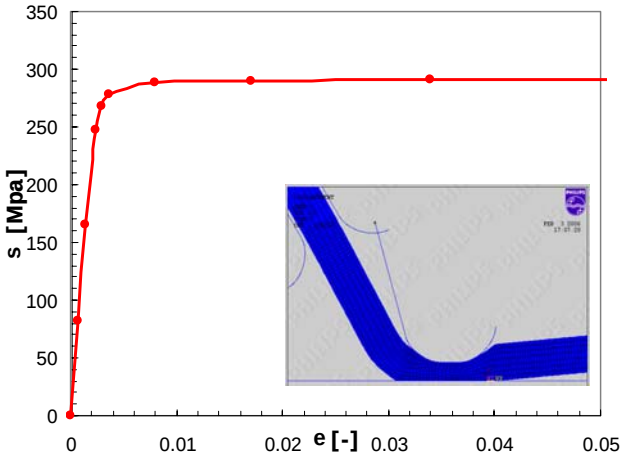

Figure 5: Measured Stress-strain curves under monotonic uni-axial tensile load is approximated with a multi-linear kinematic hardening law for the 2D model.

	ρ_{el} $\mu\Omega.mm$	$\rho.Cp$ J/mm^3	K W/mK	E GPa	ν [–]	α ppm/K
99.9% Copper	17	.0089* 0.385	390	120	0.33	17.8
Nickel	78	.0089* .439	91	213	0.3	12.9
Epoxy substrate	-	0.002* 1.6	0.3	21.5 4.82 z	0.19 0.3 xy	14 50 (z)
Aluminum	32.4+ 0.114T	.00268* 0.92	195- .059T	64	0.3	23

Table 1 Material properties used in the FE model.

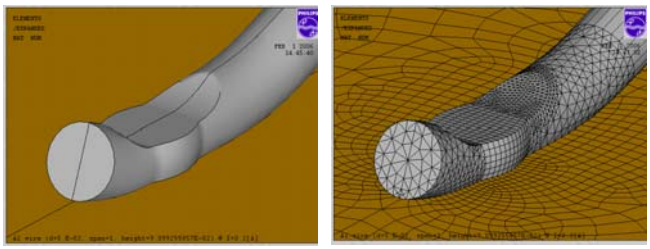

Figure 6: 3D FE model with the mechanical mesh on the right. In contrast to the mechanical model that uses a hex dominated mesh (with higher order tets), the electro-thermal model uses a tet dominated lower order mesh.

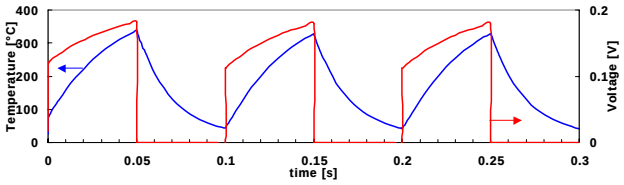

Figure 7 Simulated voltage and temperatures versus time response

To create the wire geometry, the loop shapes from the samples were measured and parameterized by 5 x-y coordinates and the 2 bond angles in order to use the actual sample geometry in the FE simulation. The two departure angles were measured in a SEM. Average parameter values of 5 samples were used in the FE model and the coordinates were fitted with a spline. The wedge of the wire bond was sculpted using simple geometric shapes, but the parameters to do this were kept constant over the different simulations. Material properties are listed in Table 1 and were taken from literature or obtained from the vendor.

To validate the model, temperatures were measured by infrared thermography on an Agema^{TM}900LW infrared scanner. This camera however, has barely sufficient resolution (20µm) to perform an accurate measurement. Electrical measurements proved more useful, and measured and simulated voltage response (Figure 7) was found to be in good agreement.

5. Results

Bonding process

The results of the simulation of the bonding process are depicted in Figure 9 through Figure 11. Although the absolute value of the (cumulative) plastic strains should not be trusted too much, it can be seen that the first bond has more than twice the plastic deformation of the second bond, which is induced by the twisting of the wire during travel-up and travel-over of the tool.

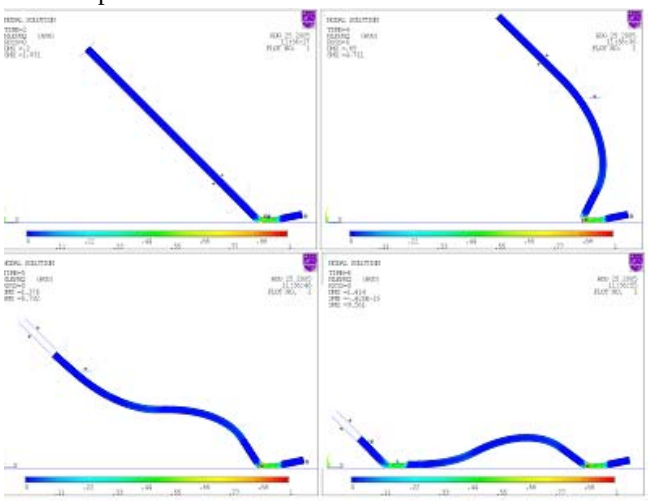

Figure 8: Initial damage is estimated using 2D FE simulations of the bonding process

This simulation was performed for al four loop shapes/settings resulting in the plastic strains in Table 2 at the end of the bonding. The average plastic strain over the width of the wire, the same 25um band as used in the stress averaging, is listed to reduce the effect of the singularity in the corner. It is interesting to see that the extremely thin wedge has no significantly increased plastic strain in the heel of the bond, but only in the foot of the bond.

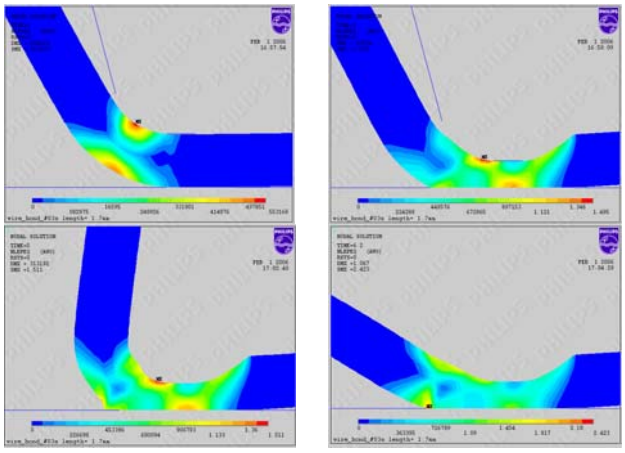

Figure 9 For the first bond four steps of the bonding process induces significant plastic strains (shown for wire#3).

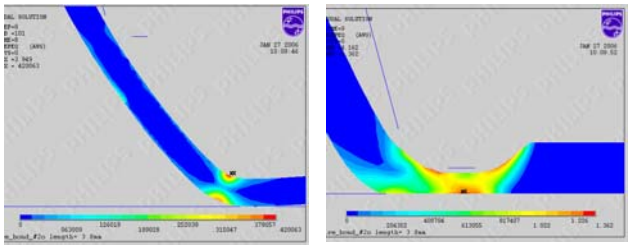

Figure 10 For the 2nd bond two steps of the bonding process induce plastic strains (shown for wire#1), the bending of the wire and the squashing of the wedge.

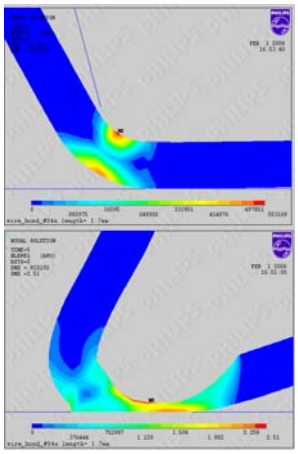

Figure 11 a,b,c: The larger plastic deformations in the thinner wedge bond is not located in a critical region for wire#4.

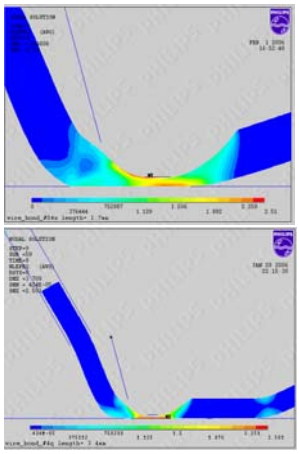

Figure 12 (11d) For the 2nd bond of wire#4 the strains are also located in a less critical region

	#1	#2	#3	#4
Bond1	1.01	1.04	1.02	1.5
Bond2	0.55	(0.55)*	(0.55)*	0.62

*Table 2 Average total accumulated plastic strain in a25µm wide band of the heel. *Is not simulated and assumed equal to #1.*

FE simulation of power cycling experiment

Since plastic deformations around microscopic defects are ultimately responsible for the damage leading to failure, the von Mises stress amplitude, averaged over the wire diameter at the heel, was used as damage metric. As a second possible damage metric the total inelastic strain was averaged over the same volume, particularly to be used for analyzing some low cycle fatigue failures during TCT.

The 3D model was used to calculate the stress amplitude in the heel of the wire. A 25µm wide band of elements was used for the averaging. This was done for three values of the current and two pulse times, in the range that was used in the test (Figure 13). For intermediate current values of the test, the results were interpolated using a power law.

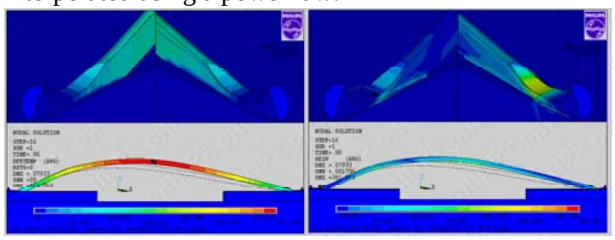

Figure 13: Temperature and von Mises stress during power cycle

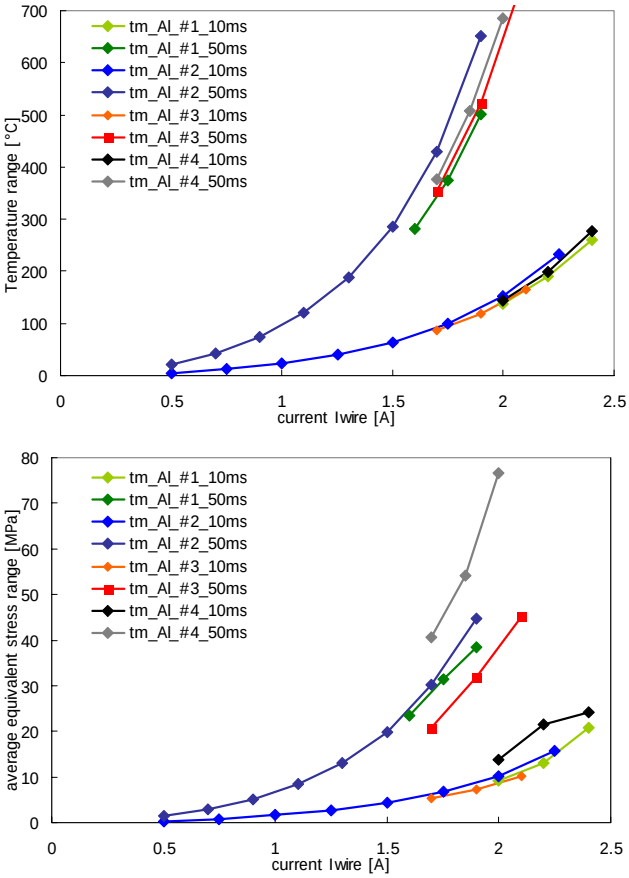

Figure 14: Simulated temperature and stress range versus current for the three different bond loops used in the test.

Life test results & failure analysis

Raw data from the life tests is depicted in Figure 15 and the cumulative distribution plot for the different stresses of wire #1 in Figure 16. Lognormal statistics were used, for the simple reason that it provided a much better fit (both in terms of r^2 and likelihood function value). In

addition, the crack growth may be considered a summation of random effects by which the central limit theorem supports the lognormal distribution.

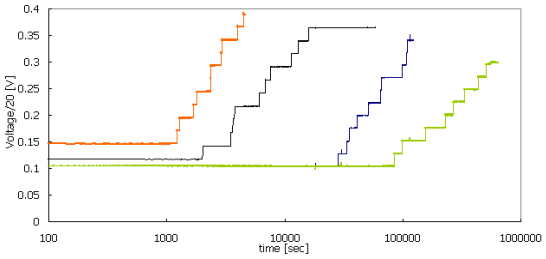

Figure 15: Raw output signal of the test: Every wire failure is indicated by a step wise increase of the voltage across the module due to the shunt diode starting to conduct current.

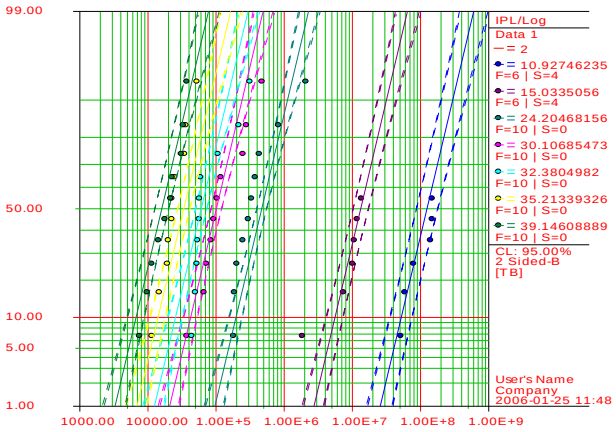

Figure 16: Lognormal cumulative distribution plot for different stress levels of wire #1.

Every failed wire was inspected after the test. Some wires showed some striation in the center of the wire where, also according to the simulations, stresses were also quite high, but the actual failure always occurred at the heel of the first bond, without any exception.

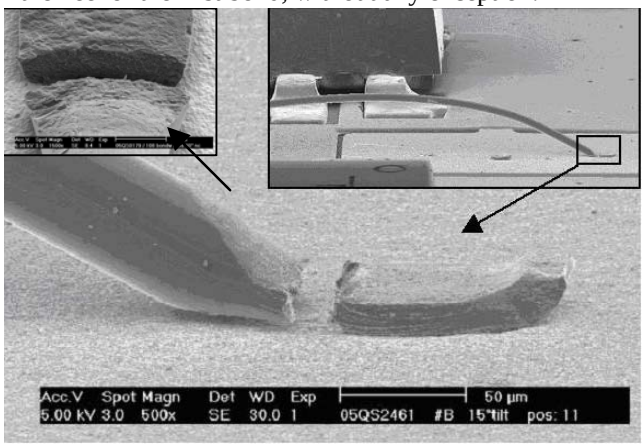

Figure 17: Fractured heel after 10^7 power cycles

Durability curves

With the simulated stress amplitudes for the different tests, the durability curves were derived using the maximum likelihood [7,8] method implemented in ALTA6 Pro [9]. The advantage of this method is that both the relevant statistical parameters as well as the parameters describing the acceleration model can be fitted simultaneously. Also, Maximum Likelihood allows withdrawn (right-censored) samples to be taken into account. Confidence bounds on reliability or time, needed when design rules are derived, were calculated using the inverse Fisher matrix to find estimates of the covariance matrix.

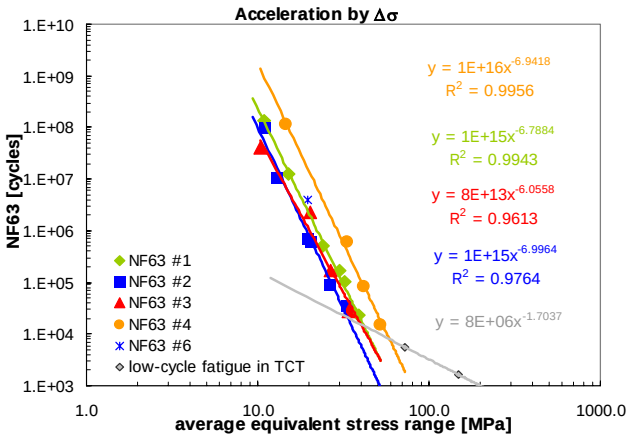

Figure 18: Extracted durability (or S-N) curve. Nf50 points of each stress level are depicted. The low cycle fatigue curve and #6 is not the same material.

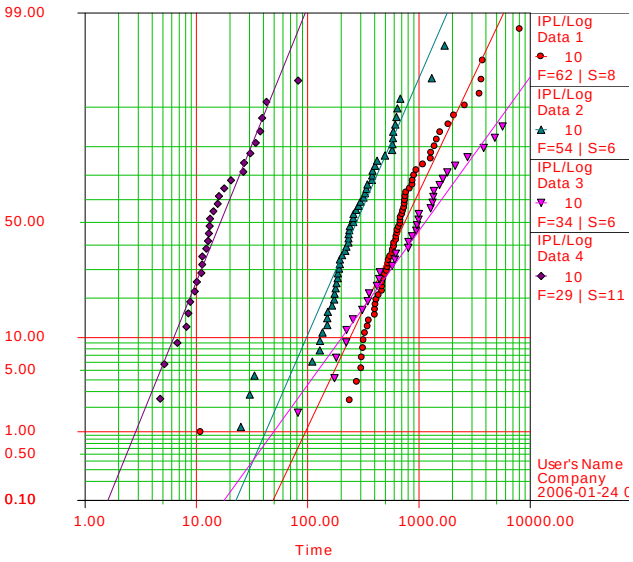

Figure 19: Cumulative distribution plots on lognormal paper scaled to the average stress used in the tests for the four different wire bonds.

Stepped stress can be analyzed in ALTA60pro with maximum likelihood method but not yet for lognormal distributions. Therefore, for lognormal distribution the effective stress (weighted time average based on Palmgren-Miner linear damage superposition principle) is used with an initial linear regression based value for C_2. The simulated stress values are used to obtain the durability plots (S-N curves) for the 4 different loop shapes depicted in Figure 18. To illustrate the different exponents for low and high cycle fatigue results of homogeneous temperature cycle test (TCT) from a

different batch and material are also displayed. Initial plastic strain for this bond was not quantified.

Life prediction & Response Surface Model

A practical application of the derived model is the prediction of the reliability in the field, or even better, deriving a design guideline for save loop geometries for a designer. A typical situation in which a design rule is needed is depicted in Figure 20. It concerns the lead to die bond that needs to be as low as possible for RF reasons. The designer will be faced with the question what bonding angle is allowed for the amount of current that will run through the wire. Therefore current and bond angle were varied for a fixed pulse length. Although additional temperature gradients (due to dissipation of the active die) can be included in the electro-thermal part of the simulation, fur the purpose of this example it was not included.

The resulting stress and TTF0.1% is depicted in Figure 21. From this graph it can either be concluded what the minimum bond angle can be, provided the design rule stress amplitude (this includes the LCL safety margins) or the most likely time to failure can be checked against the requirements.

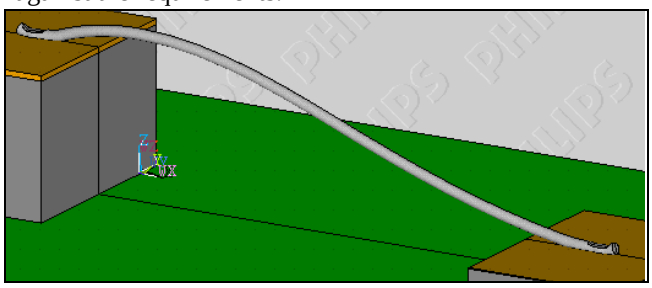

Figure 20: Example of asymmetric bond wire for which a 2-parameter RSM was derived.

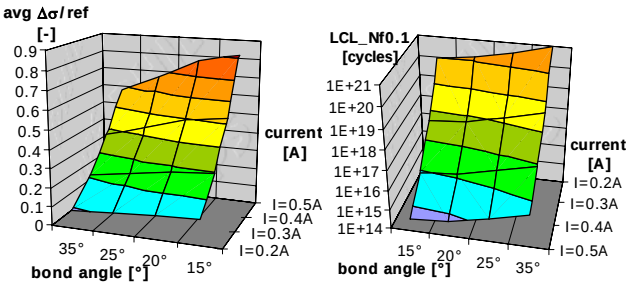

Figure 21: RSM for the asymmetric wire. Stress amplitude versus current and bond angle and lower 90% confidence bound on Nf0.1% (0.1% Failures) versus current and bond angle.

6. Discussion & Conclusions

A physics of failure approach has been demonstrated to derive a model that predicts high-cycle fatigue in aluminum bond wires. The model can be applied to derive design rules to fulfill a certain lifetime requirement or to do a reliability forecast under specified field conditions.

To study the effect of the bond process settings, durability curves were derived for four different process settings. The initial plastic strain for these settings, estimated with the 2D FE model, however turned out to be not too much different. One part of the initial hypothesis, that the durability exponent C_2 would be independent on initial damage turned out to be correct, that is it can not be discarded. The fitted exponent C_2 ranges from 6 to 7, which is in reasonable agreement with what is reported elsewhere. The offset between the curves however is actually controversy to what was expected: The samples with (slightly) higher initial damage have a better fatigue life for a fixed stress range. In the tests this sample did not perform better because stress concentration effects also subject this bond to higher stresses, so the simulated stresses being too high may already form one possible explanation. It may also be possible that this trend is true, and that work hardening actually improved the durability. This would imply that Miner's damage superposition rule might not be used over different failure modes i.e. to combine high and low cycle fatigue, which would be an interesting hypothesis to check. Additional experiments with even more different loop shape settings are therefore needed to look at this effect in more detail.

7. Acknowledgement

Special thanks go to Rafet Dumlu and Brian Peters for making the test equipment and performing the life tests.

References

1. Abhijit Dasgupta, "Probabilistic Physics of Failure Approach at the Univerity of Maryland for the Development of Reliable Electronics", Eurosime2002, Paris, 2002.
2. Hager, C., Stuck, A., Tronel, Y., Zehringer, R., Fichtner, W., "Comparison between Finite-Element and Analytical Calculations for the Lifetime Estimation of Bond Wires in IGBT Modules, ISPSO2000, Toulouse France, 2000
3. Harris, D.O. et all, "Fracture Mechanics Life Prediction for Microscale Components with Application to Wire Bonding", IEEE IRPS 1991
4. R. Fitzsimmons, E.H. Chia, "Propagation Mechanism and Metallurgical Characterization of First Bond Brittle Heel Cracks in AlSi Wire, IEEE Tran.Comp.Hybr. and Manufac. Techn., vol5, no6, 1992
5. Meyyappan, K.N., Hansen, P., McCluskey, P., "Wire flexure fatigue Model for Asymmetric Bond Height", IPACK2003, Hawaii, 2003
6. Jun Ming Hu, Michael Pecht, Abhijit Dasgupta, "A Probablistic Approach for Predicting Thermal Fatigue Life of Wire Bonding in Microelectronics", Journal of Elctr.Packaging, vol113/275,1991
7. Ohring,M, Reliability and Failure of Electronic Materials and Devices, Academic Press, 1998.
8. Paul A. Tobias, David C. Trindade, Applied Reliability, Chapmann&Hall, 1995.
9. ALTA60Pro from ReliaSoft™ User manual available through www.weibull.com or www.reliasoft.com
10. Ansys™90 theory manual, Ansys Inc.